Energy & Environmental Science

PAPER

View Article Online
View Journal | View Issue

CrossMark click for updates

Cite this: *Energy Environ. Sci.*, 2015, **8**, 995

Understanding the rate-dependent *J–V* hysteresis, slow time component, and aging in $CH_3NH_3PbI_3$ perovskite solar cells: the role of a compensated electric field†

W. Tress,* N. Marinova, T. Moehl, S. M. Zakeeruddin, Mohammad Khaja Nazeeruddin and M. Grätzel

Received 20th November 2014
Accepted 5th January 2015

DOI: 10.1039/c4ee03664f

www.rsc.org/ees

In this work we show that the rate-dependent hysteresis seen in current–voltage scans of $CH_3NH_3PbI_3$ perovskite solar cells is related to a slow field-induced process that tends to cancel the electric field in the device at each applied bias voltage. It is attributed to the build-up of space charge close to the contacts, independent of illumination and most likely due to ionic displacement, which is enhanced when the device undergoes aging. This process can also lead to a reduction of the open-circuit voltage or the steady-state photocurrent and does not directly correlate with the development of the hysteresis if it is measured at a fixed voltage sweep rate.

Broader context

Perovskite-based solar cells have emerged as a promising technology for highly efficient and low-cost photovoltaics. Despite the high efficiencies reported (20%), uncertainties remain regarding the correct measurement and reliability of these values. One source of error are very slow processes (seconds to minutes), which superimpose standard current–voltage sweeps used to determine the efficiency. A consequence of this is a hysteresis in the current–voltage characteristics when recorded under positive and negative voltage sweep rates. The reasons for the slow processes are not yet identified; neither the observed dependence on device architectures is understood. Our analysis from the device physics' point of view gives insights into the electronic and most likely ionic processes in the device during measuring current–voltage curves. Understanding and eliminating the hysteresis is not only important for a correct device characterization, but it is also essential for fabricating long-term stable devices.

A Introduction

Solar cells based on organometal halide perovskite materials have shown tremendous progress in the last five years. Starting from 3.8%, a certified power-conversion efficiency of 17.9% has been achieved and even higher values have been reported.[1–5] One major step in the development of perovskite solar cells was moving from the liquid-electrolyte-based configuration[1,6] towards an all-solid-state device.[7,8] In the meantime several technologies have been applied to fabricate perovskite thin-film solar cells either as flat films or in a mesoscopic structure using a metal-oxide scaffold. All films have a common factor in that they show a certain degree of nano-crystallinity, enabling high photovoltaic performance with low recombination constants and long charge carrier diffusion lengths in the perovskite absorber, which both harvests light and transports charge carriers.[9–11]

Ever since the emergence of highly efficient perovskite solar cells, discussions refocused on the correct measurement technique of the power-conversion efficiency.[12,13] Despite well-known protocols for correctly measuring efficiencies in the field of conventional photovoltaics (IEC60904), there is one pronounced feature in perovskite-based devices, which makes the determination of the efficiency with conventional methods ambiguous. These methods are based on measuring current–voltage curves while sweeping the voltage under a defined spectrum and specified ambient conditions (standard reporting conditions). For perovskite solar cells, however, the real, *i.e.* steady-state, current–voltage curve is difficult to determine with a conventional current–voltage scan, because it strongly depends on the voltage sweep rate for commonly used rates in the range of >100 mV s^{-1} to 1 mV s^{-1}.[12,14] Additionally, the operational point before a scan (in the dark, at open-circuit, or under short circuit) modifies the obtained results. Furthermore, the scanning direction (from positive *i.e.* open circuit, to negative *i.e.* short circuit, here denoted as backward scan) or the opposite way (forward scan) influences the obtained current–voltage curves.[4,13,15] This phenomenon results in what is called rate-dependent hysteresis, in contrast to the more persistent,

Laboratory of Photonics and Interfaces, Swiss Federal Institute of Technology (EPFL), Station 6, Lausanne, CH 1015, Switzerland. E-mail: wolfgang.tress@epfl.ch

† Electronic supplementary information (ESI) available. See DOI: 10.1039/c4ee03664f

rate-independent hysteresis. In the strict sense, only the latter is covered by the term "hysteresis". However, for simplicity, we call the observed traces in the current–voltage curve "hysteresis", keeping in mind that it is due to a very slow process lasting for seconds to minutes.

The reason for this hysteresis and the slow processes are not yet understood but are most likely attributed to the perovskite material and not to any parasitic interface effect. Hysteresis can be observed for a variety of device architectures (on TiO_2, Al_2O_3, with and without hole transport layer, *cf.* ESI†). It shows a more or less pronounced dependence on the morphology of the layers.[13,15] Several explanations have been proposed including very slow trapping and de-trapping of charges, ferroelectric behavior of the perovskite on the nanoscale,[16,17] slow ion migration, or chemical or structural changes in the material. It has further been speculated that the reason for the hysteresis might be light-induced.[12,18] So far, none of the studies goes much beyond a descriptive report of the phenomenon hysteresis. However, understanding the processes causing the hysteresis is essential to make highly efficient and long-term stable solar cells.

In this article we examine the hysteresis in the current–voltage (*J–V*) curve of mesoscopic perovskite solar cells. We investigate the *J–V* curve without the slow time component by performing fast *J–V* scans after the system has equilibrated at a given voltage point. Additionally by investigating transient photocurrents and comparing experiment to device modeling, we find that the perovskite layer tends to become field-free by screening the electric field at a wide range of applied voltages. Our observations show that this effect is independent of illumination and due to a build-up of charges at or close to the interface with the electrodes. This process is also responsible for the initial degradation of the device leading to a reduction of the photocurrent long before the absorption changes.

B Results and discussion

Dependence of *J–V* curves on sweep rate and illumination intensity

Fig. 1(a) shows current–voltage curves measured at different voltage sweep rates, starting with a backward scan and directly continuing with a forward scan. The device under investigation is fabricated by the two-step method on a mesoporous TiO_2 scaffold[2] (for details, see ESI†). The stack is fluorine doped tin oxide (FTO)/TiO_2 compact layer (approx. 30 nm)/TiO_2 mesoporous layer (250 nm)/perovskite layer (infiltrated and approx. 100 nm capping layer)/spiro-OMe-TAD (approx. 200 nm)/Au (80 nm). Depending on processing conditions, such devices show more or less pronounced hysteresis including an overshoot (bump) close to maximum power point. All devices have in common that the hysteresis becomes more pronounced with sweep rate and almost disappears for very slow scanning speed. On the other hand, the hysteresis is also reduced and finally vanishes at very high sweep rates where the slow process cannot follow. Note that the devices were kept under illumination at open-circuit before measuring. Changing the bias conditions before measuring, affects the curves significantly, in particular for higher scanning speeds. There, the bias voltage turns out to have the largest effect independent of illumination (see ESI†). However, the trends in the hysteresis remain the same. Obviously, the shape of the hysteresis depends also on how far the scan extends to negative voltages (ESI†). Besides the rate dependence, this is an additional factor that questions the usefulness of a hysteric index, which was defined in ref. 19. When measuring *J–V* curves as a function of sweep rate, it is important to comment on the exact measurement protocol and its influence on the results. In our case, we use a potentiostat (Bio-Logic SP300), where we record the current in the timespan from 50 to 100% of each voltage step. The voltage step itself is below 1 mV for scan rates <1000 mV s^{-1}. With higher scan rates, the voltage resolution decreases and less averaging results in a noisier signal, but without changed general trends. Details are found in ESI.†

In general, there are two distinct possibilities to explain the observed rate-dependent hysteresis: The discrepancy between the (quasi-)steady-state curve and the curve at faster scan rates is either due to displacement current[20] or due to a changed quasi-steady-state photocurrent generation when the device was kept at another bias voltage beforehand. The first possibility could be related to ionic movement or other processes that lead to a slow displacement of charge. *E.g.* a slow detrapping of charge could cause such a hysteresis including the bump. This charge might have been stored previously under open circuit or forward bias, which favor high charge carrier densities within the solar cell. However, all these explanations are not suitable to describe the rate-dependence of the hysteresis seen in Fig. 1(a). This is mainly due to two reasons:

First, the amount of displaced charge would be immense because the low voltage-sweep rate gives rise to a response time of several seconds where a current of several mA cm^{-2} flows. Thus assuming that only the bump in the *J–V* curve observed for the 10 mV s^{-1} sweep rate was due to displaced charge and integrating the current over that time would result in a surface charge of 30 mC cm^{-2}. In a rough estimation this corresponds to a capacitance of >10 mF cm^{-2} assuming 1 V bias whereas the geometric capacitance is supposed to be in the μF cm^{-2} range.[21] The displaced charge would correspond to an equally distributed charge concentration of 10^{22} cm^{-3} (200 nm thick layer), which is unrealistically high. A similar estimation has lead to comparable values.[13] Second, the shape of the hysteresis and the relative height of the bump are independent of light intensity as shown by using normalized *J–V* curves in Fig. 1(b). This means that the effect causing the displacement (*i.e.* some charge concentrations) need to scale with the light intensity and thus could not be introduced by charge carriers injected from the contacts under forward bias. At the same time, the photogenerated charges themselves cannot cause the hysteresis, *e.g.* by piling up and forming a space charge. Such effects would be more severe for higher illumination intensities.[22]

Thus, the second possibility remains: The *J–V* curve shows a (quasi-)steady state electronic photocurrent, where the share between charge extraction and recombination depends on the conditions the device withstood in the time preceding the scan. These conditions are not set by free charge carriers (neither from the contacts nor photogenerated), but by an additional process independent of light intensity. This explains the

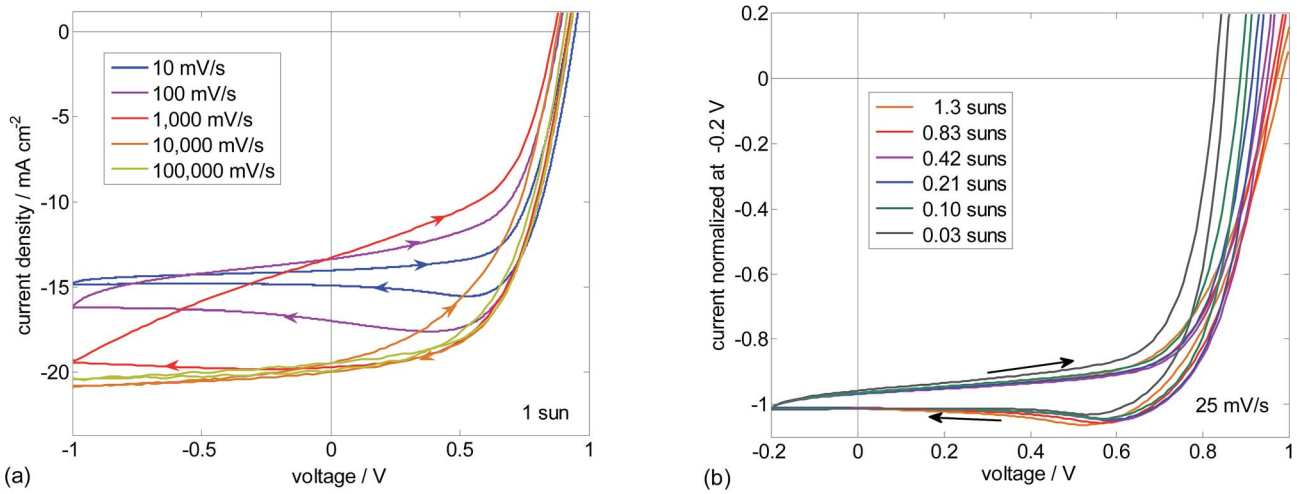

Fig. 1 Current–voltage curves of TiO_2 based $CH_3NH_3PbI_3$ devices with pronounced hysteresis. Arrows denote the sweep direction. (a) Scans with different scan rates from 1 V to −1 V and back to 1 V. Sweep rates are from 10 to 100 000 mV s^{-1} (b) *J–V* data as a function of illumination intensity normalized at −0.2 V. The shape of the hysteresis remains almost the same. Only the effect of the light intensity on the open-circuit voltage and the influence of the series resistance at high light intensities, *i.e.* photocurrents, are seen. Illumination is provided by white LEDs and the intensities stated are expressed as approximate sun equivalents for these devices.

unchanged shape of the hysteresis with light intensity and is in accordance with the fact that the current at fast sweep rates does never exceed the photocurrent possible from light absorption (approx. 22 mA cm^{-2}). It, furthermore, means that electronic processes, which are fast (<μs), generate the photocurrent, whereas the additional slow process defines the surrounding conditions. During a voltage sweep at moderate speed, these conditions are continuously and belatedly changed affecting the charge collection efficiency. As the collection efficiency is obviously higher when the device was kept at a positive bias voltage, the photocurrent can be higher close to the maximum power point compared to the short-circuit current. This results in a bump in the *J–V* curve, which, however, does not exceed current values that are possible from absorption. It occurs if the timescale of the slow process is roughly in the same order of magnitude as the time for a *J–V* scan.

Electronic *J–V* curve and compensation of the electric field

To isolate these two processes, namely charge collection as a function of voltage (denoted as electronic *J–V* curve) and changed conditions as a function of voltage, we perform the following experiment: We apply a certain bias voltage and let the device reach steady state by waiting for 30 s. Then, starting at this voltage we do a very fast *J–V* scan, which only reflects the electronic *J–V* curve, as the slow processes cannot follow. This procedure can be repeated at several voltages. The *J–V* curves obtained for starting voltages of −0.5, 0, 0.5 and 1 V are shown in Fig. 2(a). The sweep rate is chosen to be sufficiently fast to prevent the hysteresis and approximately reach a *J–V* curve that is independent of sweep rate. Too high sweep rates (here >100 000 mV s^{-1}) should be avoided as well, because they introduce electronic displacement current due to a limited RC time constant of device and measurement circuit. The inset shows that a sweep rate in the range of 50 000 to 100 000 mV s^{-1} is optimum.

The electronic *J–V* curves in Fig. 2 share one peculiarity: The photocurrent and thus the charge-collection efficiency as a function of applied voltage depends strongly on voltage close to each biasing voltage V_{preset}. The absolute photocurrent is much smaller for $V \gtrsim V_{preset}$ and much larger for $V \lesssim V_{preset}$ compared to the value expected from the steady-state photocurrent at these voltages. Consequently, the electronic *J–V* curve shows an S-shape with the turning point located close to V_{preset}. This shape is horizontally shifted with V_{preset} as seen when comparing the *J–V* curves for $V_{preset} = -0.5$ V and 0 V. Such an S-shape can be explained investigating the electric field in the device. It denotes a situation, where charges flow against an electric field when the applied voltage exceeds the voltage at the inflection point of the *J–V* curve.[23] In that case, the charges are only driven by diffusion due to selective contacts, which is inefficient if the field is reversed.

To further prove the outlined idea, we use a device simulation based on a drift-diffusion model.[24] We assume that the intrinsic perovskite is sandwiched in between selective contacts and that the electric field in the perovskite is dominated by the applied voltage minus the built-in voltage. This holds for perovskite solar cells resembling a p-i-n structure with p-doped hole transport layer, intrinsic perovskite layer, and n-type TiO_2 as recently shown experimentally.[25,26] As we model the electronic *J–V* curve only, we set the built-in potential to the negative value of V_{preset}, which corresponds to the situation where the slow process has set the electric field close to zero at each V_{preset}. Fig. 2(b) shows the simulated *J–V* curves, which reproduce the experimentally observed trends. As neither a detailed description of the process modifying the built-in potential nor the complex morphology of the layer including lateral inhomogeneities was considered, a quantitative fitting was not performed at this stage. Nevertheless, this proof of principle shows that the slow process tends to suppress the electric field in the perovskite layer.

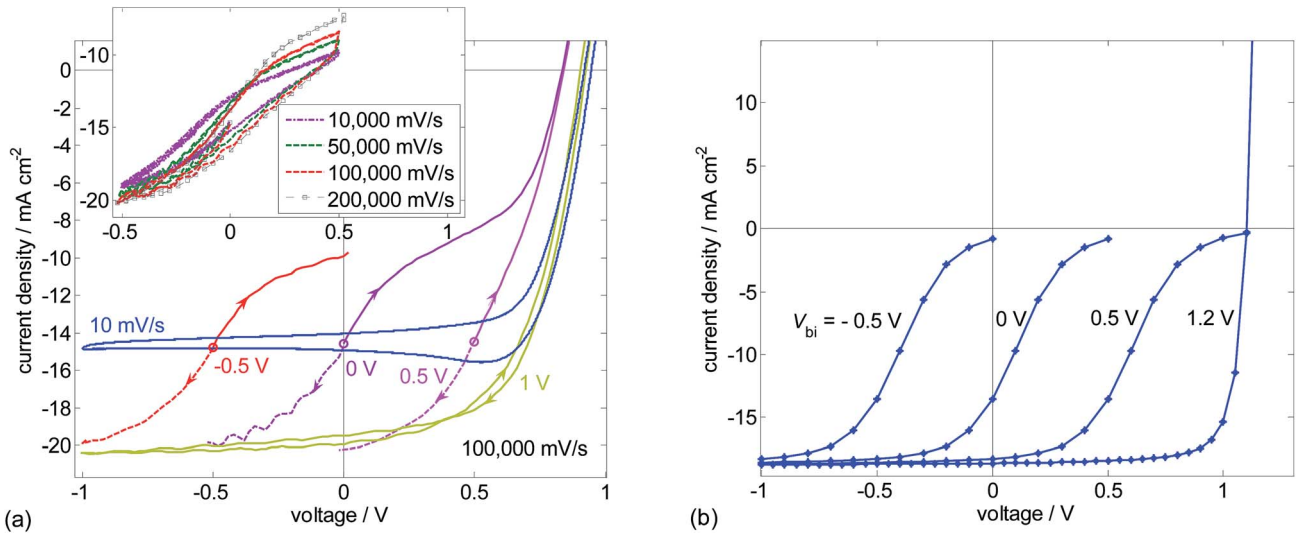

Fig. 2 (a) J–V curves after the solar cell was kept for 30 s at different starting voltages V_{preset} (−0.5, 0, 0.5, 1 V) marked by a circle. A fast scan discloses the response (electronic J–V curve) that the device has under the conditions set by V_{preset}. The inset shows the shape of the J–V curve for $V_{preset} = 0$ V, while cycling the voltage twice between −0.5 and +0.5 V. Whereas a rate of 10 000 mV s^{-1} is almost too slow, 200 000 mV s^{-1} show significant capacitive displacement current. (b) Device simulations with built-in potential $V_{bi} = -0.5$, 0.0, 0.5, 1.2 V.

A reduced built-in potential decreases the open-circuit voltage in case of non-perfectly selective contacts.[23] This explains, why devices with hysteresis (can also) show a lower open-circuit voltage for the forward scan[4,5] (*cf.* Fig. 1(a and b)). To verify the role of the contact selectivity and built-in potential, we investigate a device without the hole-blocking TiO_2 compact layer. In this case, a non-selective contact is formed between the FTO electrode and the perovskite. Indeed, Fig. 3 shows that V_{oc} for devices without blocking layer is significantly lower for forward scans at intermediate sweep rates. Furthermore, V_{oc} is strongly reduced after preconditioning the device at low bias, which decreases the built-in potential.

A reduced built-in potential of a device with non-selective contacts is expected to be seen in the dark J–V curves as well. Fig. 4 shows electronic J–V curves of a device without blocking layer in the dark. The exponential region is shifted with V_{preset} clearly indicating a modified electric field in the device. Furthermore, the dark current is not 0 at 0 V during the fast voltage sweep, but reaches 0 at $|V| \leq |V_{preset}|$. This means that the electric field is (almost) compensated by the slow process and not by charge carriers piling up.

The effect of compensating the electric potential is sketched in Fig. 5. The electric field due to the built-in potential and external bias voltage, if present, drives mobile charge carriers

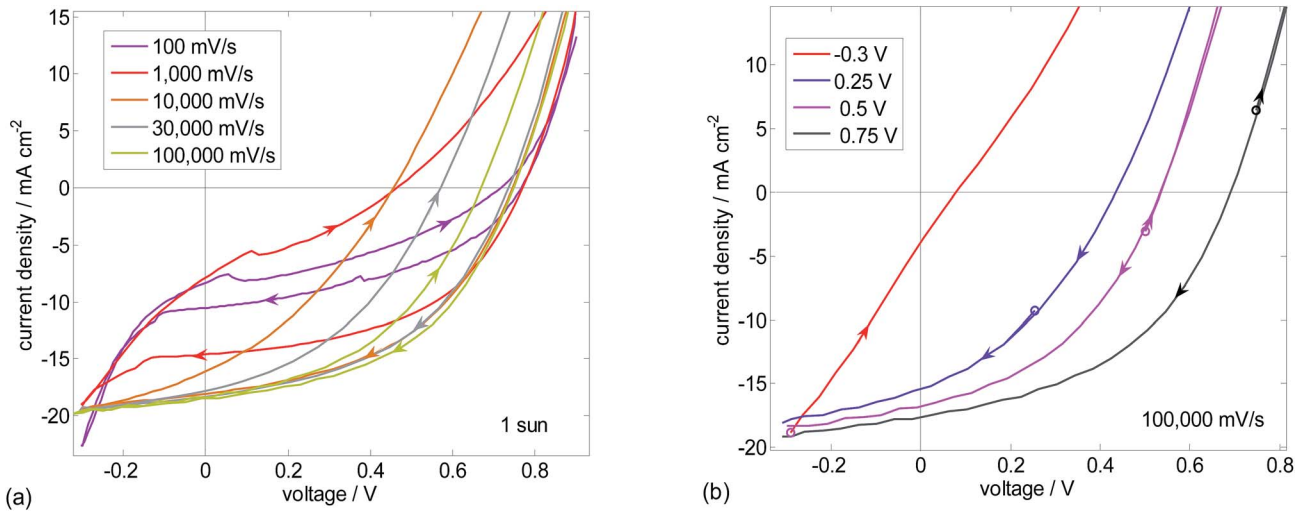

Fig. 3 J–V curves for a device without TiO_2 hole blocking layer, *i.e.* without selective electron contact (a) for different sweep rates from 0.9 V to −0.3 V and back; (b) after 10 s at different V_{preset} (−0.3, 0.25, 0.5, 0.75 V, marked by a circle). The compensation of the electric field reduces V_{oc} due to a non-selective electron contact. For low sweep rates or negative V_{preset}, the poor blocking properties below −0.1 V become obvious.

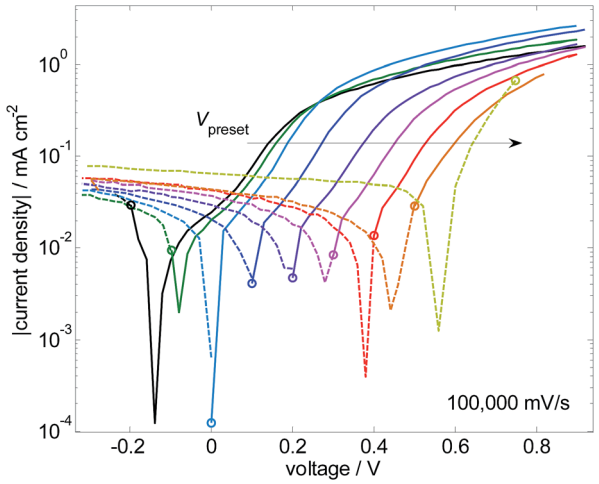

Fig. 4 Electronic J–V curves for a device without TiO_2 hole blocking layer in the dark after the device equilibrated at V_{preset}, which is marked with a circle. Solid lines are forward scans, and dashed lines denote backward scans.

towards their respective electrodes. However, if this field is compensated, charge extraction becomes less likely, in particular when a voltage larger than V_{preset} is applied in a fast scan. For non-selective contacts, V_{oc} is decreased, reaching 0 V in the extreme case due to a missing driving force for a selective charge extraction. However, quickly measured electronic J–V curves can show a $V_{oc} \neq 0$ V, if the compensation of the field is not caused by the charge carriers themselves.

Transient measurements

To further characterize the slow time component, we repeat the same measurement with the solar cell (with blocking layer) in the dark at various preset biases. This experiment shows the same results. Additionally, we monitor the transient photocurrent upon a voltage step. Response times in the range of seconds, which match reported data,[13,15,18,27] reveal the time for reaching a new steady-state photocurrent due to changed conditions. Fig. 6(a) shows the transient currents when the voltage is changed from 1 V ($\gtrsim$ open-circuit voltage) to −0.5 V. The different curves are collected under varied delay times for switching on the illumination. We see that the response is independent of whether the light was on or off while biasing with 1 V (red dots and grey line). The current shows a strong overshoot because the slow process has not yet come into play, compensating for the field in the perovskite, which has been preconditioned at 1 V beforehand. Due to the large-signal analysis, the decay is multiexponential with time constants in both the 1 s and $\gtrsim$5 s range. Whether the difference in time scales can be attributed to different processes or whether they result from the lateral inhomogeneity of the device, remains to be investigated. An ulterior switching-on of the light reduces the overshoot, but follows the tails of the curves obtained when the light was turned on earlier. Thus, the establishment of a novel steady-state situation after a change of voltage occurs in a similar way independent of whether the device is in the dark or under illumination. Consequently, this compensation of the electric field is not influenced by illumination. As already anticipated for the case of a missing hole blocking layer, it has to be provided by charge that is displaced by the applied voltage. The charge builds up close to the electrodes and screens the electric field similarly as in a conductor. The data of Fig. 6(b) enforce this interpretation: When switching the voltage at a device in the dark from 0 V to forward bias (here 1.1 V), the electrical current reaches values close to its steady-state value after less than 1 s (green line). However, the emitted photon flux increases for several tens of seconds (red line). This means that non-radiative recombination at the contacts is continuously decreasing[11] indicating the creation of a larger built-in potential under forward bias, which reduces the amount of charges that reach the wrong electrode. The transient open-circuit voltage (dashed) reflects this trend as well. It decreases in cases where the pre-bias was larger than V_{oc} (1 V) because the built-in potential is decreasing after having switched to open circuit. On the other hand, V_{oc} increases in cases where the pre-bias was lower (0 V, −1 V) than the steady-state-V_{oc} because the built-in potential is gradually increasing reducing recombination at the electrodes. All processes occur at the same time scale of seconds.

To further prove that at $V > V_{preset}$ the device works electronically in a diffusion-driven mode against a reversed field, we measure photocurrent transients in the microsecond range, where the slow processes cannot follow. These transients have

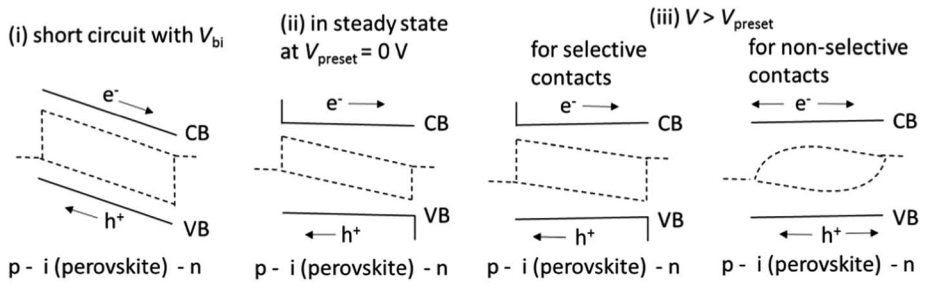

Fig. 5 Sketch of band diagrams for different situations under illumination: (i) device with (an uncompensated) built-in potential V_{bi} at short circuit, (ii) device with a compensated V_{bi} at short circuit, (iii) device of (ii) with applied positive bias, where the field in the device is detrimental for charge extraction, which is only driven by diffusion due to selective contacts. If contacts are not selective, charges diffuse to both electrodes, decreasing quasi-Fermi level splitting and V_{oc}. Quasi-Fermi levels are dashed and band bending close to and in n and p regions are neglected for simplicity.

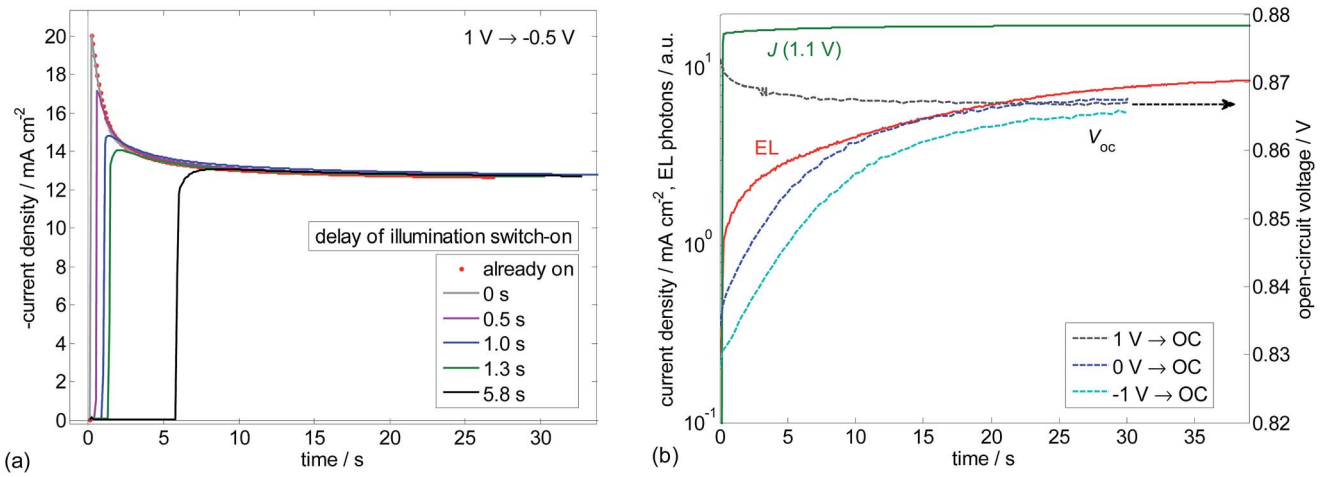

Fig. 6 (a) Slow transient photocurrent response after the voltage is switched from 1 V to −0.5 V at $t = 0$ s. The illumination is on during the whole time (red dots) or switched on later (solid lines). The light acts as a probe for the slow process which shows a response time in the range of 10 s independent of illumination. (b) Rise of the injection current J (green) and electroluminescence (EL) photon flux (red) when switching from 0 V to 1.1 V. Dashed lines are open-circuit voltage transients upon switching to open circuit after the device has been biased at the given voltages. All processes show similar time scales.

been proven valuable to find the operation regime of thin-film solar cells.[28] Before elaborating on the data series of Fig. 7 in detail, we address the general shape of the transient curves. At time $t = 0$ the light is switched on and at $t = 500$ μs the light is switched off. In a well-working device, the photocurrent rises and decays monotonically within a characteristic time span (*e.g.* the blue curve in a). However, in case of a charge extraction problem, overshoots emerge (*e.g.* the blue curve in b). In a diffusion-driven regime, the current is large directly after switching on the light before the diffusion gradient is established. Then, recombination increases due to high charge-carrier densities, leading to a decrease of the photocurrent. An overshoot can also be seen when switching off. It is due to injected charges that are delivered from the electrodes and cancel the charge carrier density, which made up the diffusion gradient. Note that these overshoots cannot be observed for devices with high photocurrents and small J–V hysteresis.

Now, we investigate the series in Fig. 7. We would expect less initial overshoots when we switch from high voltage to low voltage. In this case, the conditions are still pre-set by the previous high voltage allowing for a (high) built-in potential. Indeed, we cannot see overshoots in this situation (blue line in a). Recording transients subsequently in time, we observe that the overshoot emerges and the steady-state photocurrent decreases. This is

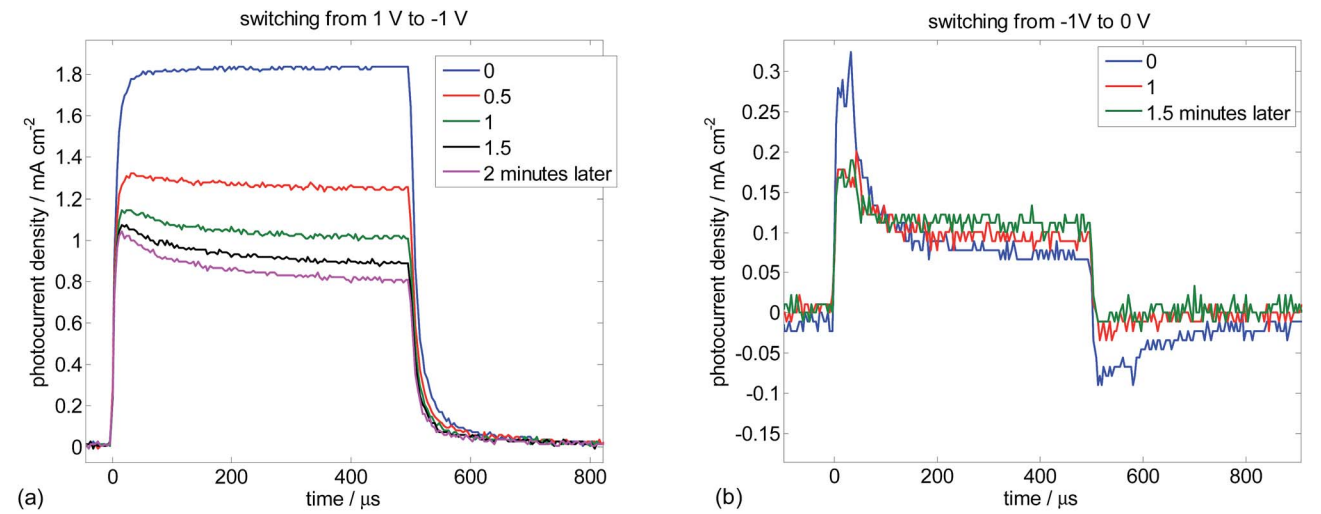

Fig. 7 Transient photocurrents, where the light (red LED) is switched on at $t = 0$ s and off after 500 μs (a) after switching from 1 to −1 V: the photocurrent decreases with time and overshoots become visible as the applied negative field is more and more compensated. (b) after switching from −1 V to 0 V: initially, strong overshoots can be seen, which decrease with time while the photocurrent increases. To avoid the millisecond response of devices based on mesoscopic TiO_2 and to exploit a pronounced slow time component, a planar configuration is used for this experiment.

consistent with the idea of a space charge built up close to the electrodes that more and more reduces the built-in field. When switching from negative to positive, the trend is inverted (b). These overshoots together with the intensity independence of the S-shape in the *J–V* curves are clear indications for a canceled field in the perovskite. This macroscopic effect makes microscopic processes in the perovskite that could influence photocurrent generation such as ferroelectric nano domains[16,17,19] unlikely.

Discussion of microscopic processes

We think that ions (vacancies and/or interstitials) are responsible for the slow process, where either positive or negative ions migrate from a location close to one surface to the other leaving behind the inverse charge. It is also possible that positive and negative ions are moving or charge-displacement is happening only close to the perovskite surface, *i.e.* at the electrode. Ions (interstitials or vacancies) move driven by a field in the perovskite layer similar to electrons and holes as sketched in Fig. 5. However, ions are not extracted at the contacts, where they pile up instead and generate a space charge. This charge counteracts the electric field leading to a reduction of the field in the bulk part of the intrinsic perovskite layer.

A giant dielectric constant[29] ε is not supposed to cause the hysteresis, as it only increases screening of charges. However, it does not modify the electric field F at a given applied bias ($F = -V/d$, with thickness d). What is observed as giant dielectric constant in that publication,[29] might be explained by the influence of slowly displaced ions on photocurrent. An alternative source for the hysteresis could be surface states which are filled dependent on the position of the Fermi level and the electric field. However, trapping of electronic charges at these states is supposed to happen on much faster timescales and is not expected to compensate for the field in the large voltage range including both signs shown in Fig. 2. Ferroelectric contributions should give rise to a delayed polarization (P) curve, which will affect the displacement field inside the material $D = \varepsilon F + P$ coming along with a surface charge on the electrodes. Since the *J–V* curves can be described by one macroscopic process, it is unlikely that ferroelectric nano domains influence the photocurrent. If there is a ferroelectric contribution, it should be macroscopic. However, if the contacts are metal-like, the remanent ferroelectric polarization leaves some surface charge on the electrodes, which guarantees that the electric field in the devices is not changed for a given V: $F = -V/d$ after dipoles have switched. As it is the electric field that drives photocurrent (and not D), ferroelectric effects can only be responsible for the hysteresis if oriented dipoles cause an extended space charge built up at non-highly conductive interface layers. In brief, the following points argue for ion migration as a non-electronic reason for the hysteresis:

- The timescale of seconds to minutes.
- The material system known as an ionic conductor.[30–33]
- The strong dependence on sweep rate and temperature.[27]
- The counterbalancing of the electric field for each applied voltage up to high negative values.
- The gradual change with the applied voltage not showing any threshold value.
- The sensitivity to fabrication and aging.

The important fact is that these ions are not strongly electronically active as recombination centers for electrons,[34] but instead decrease the charge collection efficiency by screening the field.

It is observed that the strength of the hysteresis depends on processing conditions and device architecture, where planar TiO_2 based architectures seem to be prone to stronger hysteresis.[4] On the other hand, alternative geometries and contact passivation measures seem to suppress hysteresis. We think that all these parameters govern the availability and mobility of ionic species by influencing the morphology of the perovskite layer including defects.

Hysteresis and aging

To find indications for ions we examine the device during aging. We observe that the device is stable (for weeks) under Argon atmosphere. However, photocurrent drops if the device is kept under air, where illumination accelerates the aging. Applying a bias voltage and driving current in the dark accelerates degradation as well, but to a lesser extent. The reason for the decrease of photocurrent is supposedly due to reactions of the perovskite with water (humidity), decomposing the perovskite material. The change of the color from black to yellow indicates the formation of lead iodide (PbI_2).[35] However, this change in color occurs on much larger timescales when compared to the observed reduction of the photocurrent. During aging of the device shown in Fig. 8(a), a change of the absorption of the perovskite layer cannot be observed. This is expected because a fast scan shows that the maximum photocurrent can still be generated (dashed lines). Consequently, neither absorption nor the electronic properties are significantly altered. However, the effect of the compensation of the electric field becomes more severe, affecting more regions in the device, whereas the hysteresis remains similar or is even slightly decreased at the voltage sweep rate shown (50 mV s^{-1}). Thus, the hysteresis (index) itself is not sufficient to judge the processes ongoing in the device, but a comparison of fast and slow scans is required. This becomes obvious when comparing the *J–V* curves of fresh and aged devices for different voltage sweep rates (Fig. 8(b) with Fig. 1(a)). At low sweep rates (10 to 100 mV s^{-1}) the hysteresis has almost vanished for the aged device, which, however, delivers significantly lower steady-state photocurrent. On the contrary, for high rates, it is more pronounced than for the fresh device. Consequently, the effect of the slow process is accelerated by a factor of 10 to 100, which might be due to the presence of more mobile ions.

Since this aging tends towards a decomposition of the perovskite and formation of lead iodide on the long run, we see the trends in Fig. 8(a) as an indication that degradation of CH_3NH_3I and the formation of PbI_2 and/or further reaction products can be responsible for the hysteresis and the reduced photocurrent at moderate sweep rate. Besides being created during aging, PbI_2 might be present due to a not fully completed conversion, where we observe stronger hysteresis effects. For instance, mobile iodide vacancies are expected in iodide perovskites analogously to oxygen vacancies in

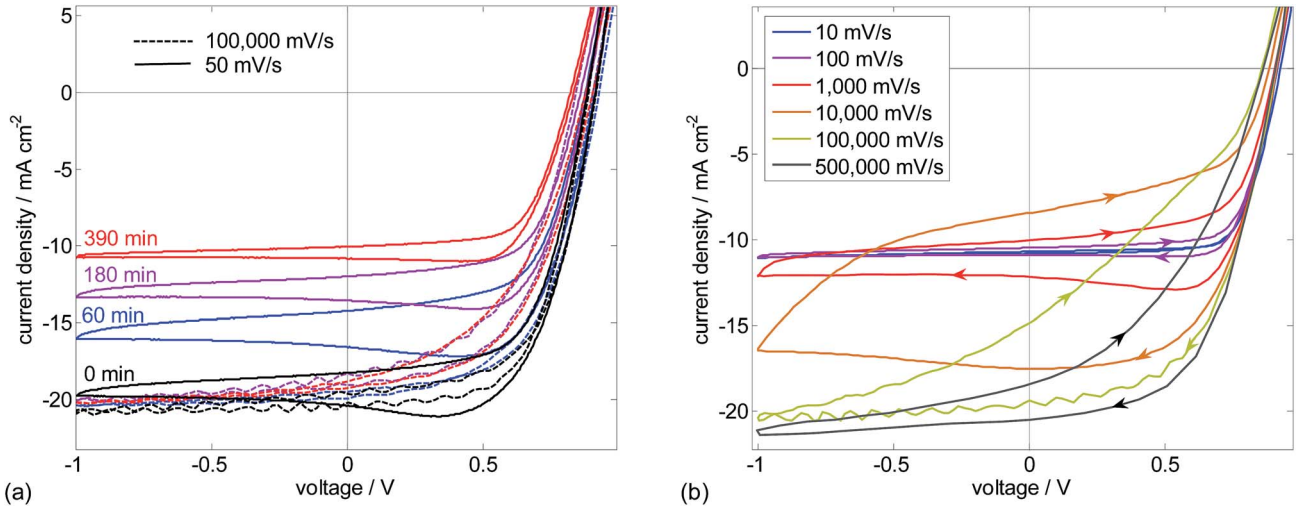

Fig. 8 (a) *J–V* curves during aging the device at atmosphere under open circuit and at 1 sun illumination provided by LEDs. Fast scans show that the source of degradation in photocurrent is not of optical or electronic nature but due to the slow time component becoming more dominant. Note that the absorption spectra are unchanged upon aging. (b) *J–V* curves of the same device as in Fig. 1(a) after aging. Compared to the fresher device, the slow time component became faster (10 to 100 times) which reduces the hysteresis at lower voltage sweep rates, but not in general.

perovskite oxides.[30,32,36] The concentrations of ionic "defects" that are required to create a significant space charge are below the range of percentages and can, thus, not easily be detected by optical or structural analysis investigations. The correlation of hysteresis and aging induced by oxygen and/or humidity is a further indication that a ferroelectric effect is unlikely. Further studies are necessary to identify the chemical changes of the perovskite close to the electrode and the dominating mobile interstitial ions or vacancies upon exposure to humidity and/or oxygen.

The experimentally observed differences between the electronic and (quasi-)steady-state *J–V* curves help to explain discrepancies in optimum layer thicknesses[37] and known diffusion lengths[10] of the charge carriers. In general, thin films are required to obtain optimal device performance, whereas the large drift and diffusion lengths of charge carriers should allow for the usage of much thicker layers for flat devices. However, due to the screening of the field, the fill factor for slow voltage-sweep rates is significantly diminished. Thus, a low photocurrent and/or fill factor in perovskite solar cells is not necessarily related to poor electronic properties.

The discussed changes in the built-in potential due to ionic displacement upon a pre-bias explain the thus far puzzling intensity (the actual pre-biasing)-dependent persistent photovoltage reported in ref. 38. The ionic displacement furthermore, might explain the persistent charge observed close to the electrodes after illumination, where the reduced electric field in the perovskite during illumination would lead to a relative displacement of positive charge towards the TiO_2.[26]

C Conclusions

We have shown that the rate-dependent hysteresis in the current–voltage curve and the strong dependence on time and sweep rate are due to charge carrier collection efficiencies that strongly depend on the built-in potential, which is modified by the applied voltage. This modification occurs in timescales of seconds to minutes and is most likely due to ions, which accumulate at the interfaces of the electrodes and screen the applied field independent of illumination. This delayed reduction of the built-in potential gives rise to the dependence of the *J–V* curve on the voltage sweep rate and direction and is responsible for the initial decrease of photocurrent upon aging the device. The differences in the hysteresis for various device architectures and upon aging can be explained by different amounts of defects in the perovskite. Although using a thin mesoscopic perovskite layer with a conductive scaffold reduces the detrimental effect of a macroscopically screened electric field, ion (vacancy) migration should be avoided for high longterm stability.

Acknowledgements

We thank Joël Teuscher and Nicolas Tetreault for providing us with vacuum processed perovskite samples and Carole Grätzel for commenting on the manuscript. The research leading to these results has received funding from the European Union Seventh Framework Programme [FP7/2007–2013] under grant agreement no. 604032 of the MESO project. S.M.Z. and M.N. acknowledge a Sciex fellowship under Project Code: 12.249. M.G. thanks the European Research Council (ERC) for financial support under the advanced research grant (ARG 247404) "Mesolight".

Notes and references

1 A. Kojima, K. Teshima, Y. Shirai and T. Miyasaka, Organometal Halide Perovskites as Visible-Light Sensitizers for Photovoltaic Cells, *J. Am. Chem. Soc.*, 2009, **131**, 6050–6051.

2 J. Burschka, *et al.*, Sequential deposition as a route to high-performance perovskite-sensitized solar cells, *Nature*, 2013, **499**, 316–319.
3 N.-G. Park, Organometal Perovskite Light Absorbers Toward a 20% Efficiency Low-Cost Solid-State Mesoscopic Solar Cell, *J. Phys. Chem. Lett.*, 2013, **4**, 2423–2429.
4 N. J. Jeon, *et al.*, Solvent engineering for high-performance inorganic–organic hybrid perovskite solar cells, *Nat. Mater.*, 2014, **13**, 897–903.
5 H. Zhou, *et al.*, Interface engineering of highly efficient perovskite solar cells, *Science*, 2014, **345**, 542–546.
6 J.-H. Im, C.-R. Lee, J.-W. Lee, S.-W. Park and N.-G. Park, 6.5% efficient perovskite quantum-dot-sensitized solar cell, *Nanoscale*, 2011, **3**, 4088–4093.
7 H.-S. Kim, *et al.*, Lead Iodide Perovskite Sensitized All-Solid-State Submicron Thin Film Mesoscopic Solar Cell with Efficiency Exceeding 9%, *Sci. Rep.*, 2012, **2**, 591.
8 M. M. Lee, J. Teuscher, T. Miyasaka, T. N. Murakami and H. J. Snaith, Efficient Hybrid Solar Cells Based on Meso-Superstructured Organometal Halide Perovskites, *Science*, 2012, **338**, 643–647.
9 G. Xing, *et al.*, Long-Range Balanced Electron- and Hole-Transport Lengths in Organic–Inorganic $CH_3NH_3PbI_3$, *Science*, 2013, **342**, 344–347.
10 S. D. Stranks, *et al.*, Electron-Hole Diffusion Lengths Exceeding 1 Micrometer in an Organometal Trihalide Perovskite Absorber, *Science*, 2013, **342**, 341–344.
11 W. Tress, *et al.*, Predicting the Open-Circuit Voltage of $CH_3NH_3PbI_3$ Perovskite Solar Cells Using Electroluminescence and Photovoltaic Quantum Efficiency Spectra: the Role of Radiative and Non-Radiative Recombination, *Adv. Energy Mater.*, 2014, DOI: 10.1002/aenm.201400812.
12 A. Dualeh, *et al.*, Impedance Spectroscopic Analysis of Lead Iodide Perovskite-Sensitized Solid-State Solar Cells, *ACS Nano*, 2014, **8**, 362–373.
13 E. L. Unger, *et al.*, Hysteresis and transient behavior in current–voltage measurements of hybrid-perovskite absorber solar cells, *Energy Environ. Sci.*, 2014, **7**, 3690–3698.
14 H. J. Snaith, *et al.*, Anomalous Hysteresis in Perovskite Solar Cells, *J. Phys. Chem. Lett.*, 2014, **5**, 1511–1515.
15 H.-S. Kim and N.-G. Park, Parameters Affecting I–V Hysteresis of $CH_3NH_3PbI_3$ Perovskite Solar Cells: Effects of Perovskite Crystal Size and Mesoporous TiO_2 Layer, *J. Phys. Chem. Lett.*, 2014, 2927–2934, DOI: 10.1021/jz501392m.
16 J. M. Frost, K. T. Butler and A. Walsh, Molecular ferroelectric contributions to anomalous hysteresis in hybrid perovskite solar cells, *APL Mater.*, 2014, **2**, 081506.
17 Y. Kutes, *et al.*, Direct Observation of Ferroelectric Domains in Solution-Processed $CH_3NH_3PbI_3$ Perovskite Thin Films, *J. Phys. Chem. Lett.*, 2014, **5**, 3335–3339.
18 R. Gottesman, *et al.*, Extremely Slow Photoconductivity Response of $CH_3NH_3PbI_3$ Perovskites Suggesting Structural Changes under Working Conditions, *J. Phys. Chem. Lett.*, 2014, **5**, 2662–2669.
19 R. S. Sanchez, *et al.*, Slow Dynamic Processes in Lead Halide Perovskite Solar Cells. Characteristic Times and Hysteresis, *J. Phys. Chem. Lett.*, 2014, **5**, 2357–2363.
20 G. Friesen and H. A. Ossenbrink, Capacitance effects in high-efficiency cells, *Sol. Energy Mater. Sol. Cells*, 1997, **48**, 77–83.
21 N. Onoda-Yamamuro, T. Matsuo and H. Suga, Dielectric study of $CH_3NH_3PbX_3$ (X = Cl, Br, I), *J. Phys. Chem. Solids*, 1992, **53**, 935–939.
22 W. Tress and O. Inganäs, Simple experimental test to distinguish extraction and injection barriers at the electrodes of (organic) solar cells with S-shaped current–voltage characteristics, *Sol. Energy Mater. Sol. Cells*, 2013, **117**, 599–603.
23 W. Tress, K. Leo and M. Riede, Influence of Hole-Transport Layers and Donor Materials on Open-Circuit Voltage and Shape of *I–V* Curves of Organic Solar Cells, *Adv. Funct. Mater.*, 2011, **21**, 2140–2149.
24 W. Tress, *Organic Solar Cells – Theory, Experiment, and Device Simulation*, at http://www.springer.com/materials/optical+%26+electronic+materials/book/978-3-319-10096-8.
25 A. Guerrero, E. J. Juarez-Perez, J. Bisquert, I. Mora-Sero and G. Garcia-Belmonte, Electrical field profile and doping in planar lead halide perovskite solar cells, *Appl. Phys. Lett.*, 2014, **105**, 133902.
26 V. W. Bergmann, *et al.*, Real-space observation of unbalanced charge distribution inside a perovskite-sensitized solar cell, *Nat. Commun.*, 2014, **5**, 5001.
27 L. K. Ono, S. R. Raga, S. Wang, Y. Kato and Y. Qi, Temperature-dependent hysteresis effects on perovskite-based solar cells, *J. Mater. Chem. A*, 2014, DOI: 10.1039/c4ta04969a.
28 W. Tress, S. Corvers, K. Leo and M. Riede, Investigation of Driving Forces for Charge Extraction in Organic Solar Cells: Transient Photocurrent Measurements on Solar Cells Showing S-Shaped Current–Voltage Characteristics, *Adv. Energy Mater.*, 2013, **3**, 873–880.
29 E. J. Juarez-Perez, *et al.*, Photoinduced Giant Dielectric Constant in Lead Halide Perovskite Solar Cells, *J. Phys. Chem. Lett.*, 2014, 2390–2394, DOI: 10.1021/jz5011169.
30 J. Mizusaki, K. Arai and K. Fueki, Ionic conduction of the perovskite-type halides, *Solid State Ion.*, 1983, **11**, 203–211.
31 M. Maeda, M. Hattori, A. Hotta and I. Suzuki, Dielectric Studies on $CH_3NH_3PbX_3$ (X = Cl and Br) Single Cystals, *J. Phys. Soc. Jpn.*, 1997, **66**, 1508–1511.
32 H. Iwahara, in *Perovskite Oxide for Solid Oxide Fuel Cells*, ed. T. Ishihara, Springer US, 2009, pp. 45–63, http://link.springer.com/chapter/10.1007/978-0-387-77708-5_3.
33 N. Pellet, *et al.*, Mixed-Organic-Cation Perovskite Photovoltaics for Enhanced Solar-Light Harvesting, *Angew. Chem., Int. Ed.*, 2014, **53**, 3151–3157.
34 J. Kim, S.-H. Lee, J. H. Lee and K.-H. Hong, The Role of Intrinsic Defects in Methylammonium Lead Iodide Perovskite, *J. Phys. Chem. Lett.*, 2014, 1312–1317, DOI: 10.1021/jz500370k.
35 G. Niu, *et al.*, Study on the stability of $CH_3NH_3PbI_3$ films and the effect of post-modification by aluminum oxide in all-

solid-state hybrid solar cells, *J. Mater. Chem. A*, 2013, **2**, 705–710.

36 T. Ishigaki, S. Yamauchi, K. Kishio, J. Mizusaki and K. Fueki, Diffusion of oxide ion vacancies in perovskite-type oxides, *J. Solid State Chem.*, 1988, **73**, 179–187.

37 M. Liu, M. B. Johnston and H. J. Snaith, Efficient planar heterojunction perovskite solar cells by vapour deposition, *Nature*, 2013, **501**, 395–398.

38 A. Baumann, *et al.*, Persistent photovoltage in methylammonium lead iodide perovskite solar cells, *APL Mater.*, 2014, **2**, 081501.